2016

General synthesis of porous mixed metal oxide hollow spheres with enhanced supercapacitive properties

Qinghong Wang
University of Wollongong, qwang@uow.edu.au

Yuxuan Zhu
Xuzhou Normal University

Jing Xue
Xuzhou Normal University

Xinsheng Zhao
Jiangsu Normal University

Zaiping Guo
University of Wollongong, zguo@uow.edu.au

See next page for additional authors

Publication Details

Wang, Q., Zhu, Y., Xue, J., Zhao, X., Guo, Z. & Wang, C. (2016). General synthesis of porous mixed metal oxide hollow spheres with enhanced supercapacitive properties. ACS Applied Materials and Interfaces, 8 (27), 17226-17232.

General synthesis of porous mixed metal oxide hollow spheres with enhanced supercapacitive properties

Abstract
Porous mixed metal oxide (MMO) hollow spheres present high specific surface areas, abundant electrochemically active sites, and outstanding electrochemical properties, showing potential applications in energy storage. A hydro/solvothermal process, followed by a calcination process, can be a viable method for producing uniform porous metal oxide hollow spheres. Unfortunately, this method usually involves harsh synthetic conditions such as high temperature and intricate processing. Herein, we report a general and facile "ion adsorption-annealing" approach for the fabrication of uniform porous MMO hollow spheres. The size and shell thickness of the as-obtained hollow spheres can be adjusted by the carbohydrate sphere templates and the solution concentration. Electrochemical measurements of the MMO hollow spheres demonstrate excellent supercapacitive properties, which may be due to the small size, ultrathin shells, and fine porous structure.

Disciplines
Engineering | Physical Sciences and Mathematics

Publication Details
Wang, Q., Zhu, Y., Xue, J., Zhao, X., Guo, Z. & Wang, C. (2016). General synthesis of porous mixed metal oxide hollow spheres with enhanced supercapacitive properties. ACS Applied Materials and Interfaces, 8 (27), 17226-17232.

Authors
Qinghong Wang, Yuxuan Zhu, Jing Xue, Xinsheng Zhao, Zaiping Guo, and Chao Wang

General Synthesis of Porous Mixed Metal Oxide Hollow Spheres with Enhanced Supercapacitive Properties

Qinghong Wang,[†,‡] *Yuxuan Zhu,*[†] *Jing Xue,*[†] *Xinsheng Zhao,*[§] *Zaiping Guo,*[*,‡] *and Chao Wang*[*,†]

[†]School of Chemistry and Chemical Engineering, Jiangsu Key Laboratory of Green Synthetic Chemistry for Functional Materials, Jiangsu Normal University, Xuzhou, Jiangsu 221116, China

[‡]Institute for Superconducting & Electronic Materials, University of Wollongong, Wollongong, NSW 2522, Australia

[§]Hydrogen energy laboratory, School of Physics and Electronic Engineering, Jiangsu Normal University, Xuzhou, Jiangsu 221116, China

KEYWORDS: Mixed metal oxides, Porous hollow spheres, Ion adsorption-annealing process, Electrochemical properties, Supercapacitor

ABSTRACT: Porous mixed metal oxide (MMO) hollow spheres present high specific surface areas, abundant electrochemically active sites and outstanding electrochemical properties, showing potential applications in energy storage. A hydro/solvothermal process followed by a calcination process can be a viable method for producing uniform porous metal oxide hollow spheres. Unfortunately, this method usually involves harsh synthetic conditions such as high temperature and intricate processing. Herein, we report a general and facile "ion adsorption-

annealing" approach for the fabrication of uniform porous MMO hollow spheres. The size and shell thickness of the as-obtained hollow spheres can be adjusted by the carbohydrate sphere templates and the solution concentration. Electrochemical measurements of the MMO hollow spheres demonstrate excellent supercapacitive properties, which may be due to the small size, ultrathin shells and fine porous structure.

1. INTRODUCTION

Transition metal oxides have been considered to be promising electrode materials for energy storage devices such as electrochemical capacitors (ECs), fuel cells (FCs) and lithium ion batteries (LIBs). Among them, cobalt oxides exhibit outstanding anodic performance.[1-4] Nevertheless they often suffer from high cost and toxicity, as well as poor conductivity. To solve these problems, much effort is being directed towards the fabrication of cheap and eco-friendly mixed metal oxides (MMOs) like $ZnCo_2O_4$,[5-7] $NiFe_2O_4$,[8-10] Zn_2SnO_4 and $ZnSnO_3$.[11,12] Due to their complex chemical compositions, as well as the synergetic effects between two metals, MMO present higher electrochemical activity than their corresponding single metal oxides.[13-16] Unfortunately, poor conductivity and structural collapse are still severe weakness that limit full electrochemical reactions, resulting in fast capacity decay. Many approaches, such as controlling nanostructures[17-20] and synthesizing MMO/Ni substrates[21-23] and MMO/carbon hybrids[24-26] have been developed to further improve their electrochemical performance.

Hollow spheres, especially those with porous nanostructures, have attracted numerous research efforts in the energy storage field. Compared with the same-sized solid nanomaterials, hollow spheres deliver short ion diffusion paths, abundant active sites for reactions, and plentiful buffer space to accommodate volume changes during charge-discharge processes.[27-29] In recent years, much effort has been directed towards exploring effective strategies for the fabrication of

porous hollow spheres. Using carbohydrate spheres (CSs) as hard templates has been a popular method to prepare hollow spheres because they are simple in preparation yet effective in morphology controlling.[30,31] Zhang et al. prepared hollow mixed metal oxides with multiple shells by a "penetration-solidification-annealing" process.[32] The solidification process was carried out at 170 ^{o}C by refluxing to obtain M-glycolate-CSs precursor. Tian et al. prepared hollow ZnO by a hydrothermal process to obtain Zn-CSs precursor and a following annealing process to obtain ZnO product.[33] It should be noted that both the refluxing process and the hydrothermal process employed to obtain the M-CSs precursor suffer from high temperature and complicated processing. So, a facile and general strategy for fabricating porous MMO hollow spheres is highly desirable.

To solve this problem, we have developed a facile and general "ion adsorption-annealing" method which involves an ion adsorption process to prepare M-M-CSs precursor, combined with a subsequent calcination process to synthesize uniform porous MMO hollow spheres. In this method, the ion adsorption process was carried out at room temperature without any complex agents, precipitants, or surfactants, which makes it quite simple. Furthermore, the hollow structure, thin shell, and porosity endow the MMO samples with high specific surface area, good ion/electron transport properties, and volume buffer capability, which are all beneficial to the high discharge capacitance, excellent rate performance and long cycle life.

2. EXPERIMENTAL METHODS

2.1. Synthesis

The carbohydrate spheres template was prepared by the polymerization reaction of glucose under hydrothermal conditions at 180 ^{o}C for 10 h.

Synthesis of porous $ZnCo_2O_4$ hollow spheres. For the synthesis of porous $ZnCo_2O_4$ hollow spheres, 0.05 g of freshly-prepared CSs were dispersed into 50 ml of deionized water containing 0.04 mol of $Co(NO_3)_2 \cdot 6H_2O$ and 0.02 mol of $Zn(NO_3)_2 \cdot 6H_2O$ by sonication. After ultrasonic dispersion for 2 h, the resulting suspension was stirred for 12 h at 25 ℃. Then, the Zn-Co-CSs precursor was obtained after filtration, washed with DI water and dried at 60 ℃ overnight. Finally, the precursor was heated in air at 450 ^oC for 2 h with a heating rate of 1 $^oC\ min^{-1}$ to synthesize the porous $ZnCo_2O_4$ hollow spheres.

Synthesis of porous $NiFe_2O_4$ hollow spheres. 0.05 g of freshly-prepared CSs, 0.04 mol of $Fe(NO_3)_3 \cdot 9H_2O$ and 0.02 mol of $Ni(NO_3)_2 \cdot 6H_2O$ were used as the raw materials, while the other conditions were the same as the above procedure.

Synthesis of porous $ZnSnO_3$ hollow spheres. For the synthesis of porous $ZnSnO_3$ hollow spheres, 0.03 mol of $SnCl_4 \cdot 5H_2O$ and 0.03 mol of $Zn(NO_3)_2 \cdot 6H_2O$ were used as the sources of cations and absolute ethanol was used as the solvent, while the other conditions were the same as the preparation process of $ZnCo_2O_4$ and $NiFe_2O_4$.

2.2 Materials characterization

Crystallographic information of the as-prepared precursors and MMO products was obtained by powder X-ray diffraction (XRD) analysis using a Rigaku D/Max-2500 with Cu Kα radiation (λ=0.15418 nm). The morphologies and structures of the as-prepared MMO hollow spheres were investigated by scanning electron microscopy (SEM, JEOL JSM-6700F), transmission electron microscope (TEM) and high-resolution TEM (HRTEM, Tecnai G2 F20). The element analysis of the as-obtained samples was evaluated using an energy dispersive X-ray spectroscopy (EDS, Oxford ISIS300). Thermogravimetric analysis (TGA) of the as-prepared Zn-Co-CSs precursor was conducted in air up to 700 ℃ on a Q5000 thermal analyzer (TA Instruments). Nitrogen

adsorption-desorption isotherms of the MMO hollow spheres were carried out at 77 K on a Quantachrome Autosorb-IQ2 analyzer. Specific surface areas of the samples were measured by Brunauer-Emmett-Teller analysis.

2.3. Electrochemical measurements

The working electrodes were fabricated from viscous slurry containing active materials (80 wt%), acetylene black (10 wt%) and polyvinylidene fluoride (PVDF, 10 wt%) in N-methylpyrrolidinone (NMP). Then the obtained slurry was pasted onto 1 cm × 1 cm current collectors. The average loading mass was about 3 mg cm^{-2}. For electrochemical measurements, a three-electrode cell was fabricated using a Pt plate as the counter electrode and Hg/HgO electrode as the reference electrode. For $ZnCo_2O_4$ and $NiFe_2O_4$ electrodes, a 2 M KOH aqueous solution was used as electrolyte. For $ZnSnO_3$ electrode, a 1 M Na_2SO_4 aqueous solution was the electrolyte. Electrochemical properties of the electrodes were characterized by galvanostatic charge-discharge measurements (LAND battery test instrument) at various current densities and cyclic voltammetry (CV, CHI600e electrochemical workstation) tests at different scan rates. An asymmetric supercapacitor (ASC) is constructed using $ZnCo_2O_4$ electrode as the positive electrode, active carbon electrode as the negative electrode and a 2 M KOH aqueous solution as electrolyte. The two electrodes were separated using a polypropylene sheet. All electrochemical tests were performed at room temperature.

The specific capacitance C (F g^{-1}) was derived from galvanostatic charge-discharge curves using Eq. (1):

$$C = \frac{I\Delta t}{m\Delta V} \qquad (1)$$

where I (A), Δt (s), m (g) and ΔV (V) represent the charge/discharge current, the discharge time, the mass of electroactive material and the working voltage window, respectively. The energy density E (Wh kg^{-1}) and power density P (W kg^{-1}) is calculated from the following formulas:

$$E = \frac{1}{2} C_{\text{cell}} \Delta V^2 \quad (2)$$

$$P = \frac{E}{\Delta t} \quad (3)$$

where C_{cell} (F g^{-1}) is the specific capacitance of the ASC device, ΔV (V) indicates the working potential window and Δt (s) denotes the time for full discharge.

3. RESULTS AND DISCUSSION

3.1. Material characterization and probable formation mechanism

The "ion adsorption-annealing" process for porous MMO hollow spheres is illustrated in Scheme 1. First, CSs about 400 nm in diameter with smooth surfaces were synthesized (Figure S1, Figure S2a and S2b). It is well-known that abundant oxygenic functional groups, such as C=O, COOH and OH, are exposed on freshly-prepared CSs, which could adsorb metal cations by electrostatic adsorption to form M-M-CSs precursor,[30,31,34] which shows a rougher surface than the CSs (Figure S2c and S2d). The metal cations absorbed on CSs were then annealed at a certain temperature to remove the CSs templates, and uniform MMO hollow spheres with fine porous structures were obtained. The thermal properties of the M-M-CSs precursor were investigated via TGA to explore the crystallization temperature of MMO and the temperature for the removal of CSs. For Zn-Co-CSs precursor, the thermal decomposition consists of two steps (Figure S3). The first stage below 200 ℃ may be mainly resulted from the removal of physically adsorbed water. While the second stage between 200 and 400 ℃ is ascribed to the degradation of CSs coupled with the formation of $ZnCo_2O_4$. Thus, 450 ℃ was set as the calcination temperature for the transformation from Zn-Co-CSs precursor to porous $ZnCo_2O_4$ hollow spheres.

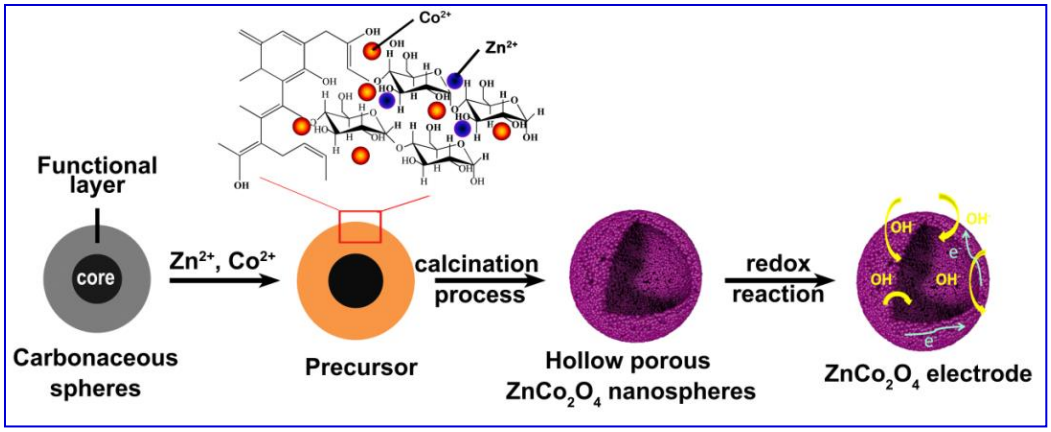

Scheme 1. Scheme for the synthesis and energy storage process for the as-prepared porous MMO hollow spheres ($ZnCo_2O_4$ as an example).

The crystal structure and morphology of the as-obtained porous $ZnCo_2O_4$, $NiFe_2O_4$ and $ZnSnO_3$ hollow spheres were characterized by XRD, SEM and TEM. Figure 1a exhibits the XRD pattern of the $ZnCo_2O_4$ product. All diffraction peaks can be attributed to cubic $ZnCo_2O_4$ phase with lattice constants of a = b = c = 8.095 Å (space group Fd3m, JCPDS 23-1390). So it is confirmed that after calcination at 450 ℃, Zn-Co-CSs precursor is fully transferred into $ZnCo_2O_4$ with high purity and good crystallinity. An SEM image displayed in Figure 1b reveals that the $ZnCo_2O_4$ sample is mainly composed of uniform hollow spheres about 200 nm in diameter. It is noted that the size of $ZnCo_2O_4$ is smaller than that of the Zn-Co-CSs precursor, indicating that the spheres have become slightly shrunken during the transformation process from the precursor to $ZnCo_2O_4$. Moreover, it is observed that the surface of the $ZnCo_2O_4$ microspheres is made up of many sintered $ZnCo_2O_4$ nanoparticles with the size of tens of nanometers. The hollow feature is further confirmed by the TEM results shown in Figure 1c. Further TEM analysis (Figure 1d) reveals that the $ZnCo_2O_4$ spheres possess an ultrathin shell (about 20 nm in thickness) composed of nanoparticles about several nanometers in size, among which numerous mesopores have been

generated. TEM images clearly show the porous structure of the $ZnCo_2O_4$ spheres, which may be caused by rapid mass transport through the shell during calcination. A more detailed HRTEM image shown in Figure 1e presents clear lattice fringes with interplanar distances of 0.24 nm, 0.29 nm and 0.47 nm, corresponding to the (311), (220) and (111) planes of spinel $ZnCo_2O_4$, respectively. It is observed that the selected area electron diffraction (SAED) pattern displays well-defined rings (Figure 1f), demonstrating the polycrystalline nature of the $ZnCo_2O_4$ hollow spheres. Moreover, the molar ratio of Zn: Co: O from the EDS spectrum (Figure S4) is ~1: 2: 4 within the samples, further confirming the formation of $ZnCo_2O_4$ pure phase. The porosity and specific surface area of the $ZnCo_2O_4$ hollow spheres were characterized by N_2 adsorption/desorption isotherms and pore size distribution measurements. Figure 2b exhibits a pore size distribution in the range of 2 to 5 nm, which agrees well with what can be observed in the TEM images. It is calculated that the pore volume is 0.44 $cm^3\ g^{-1}$. Remarkably, the porous $ZnCo_2O_4$ hollow spheres display a specific surface area of 172.62 $m^2\ g^{-1}$.

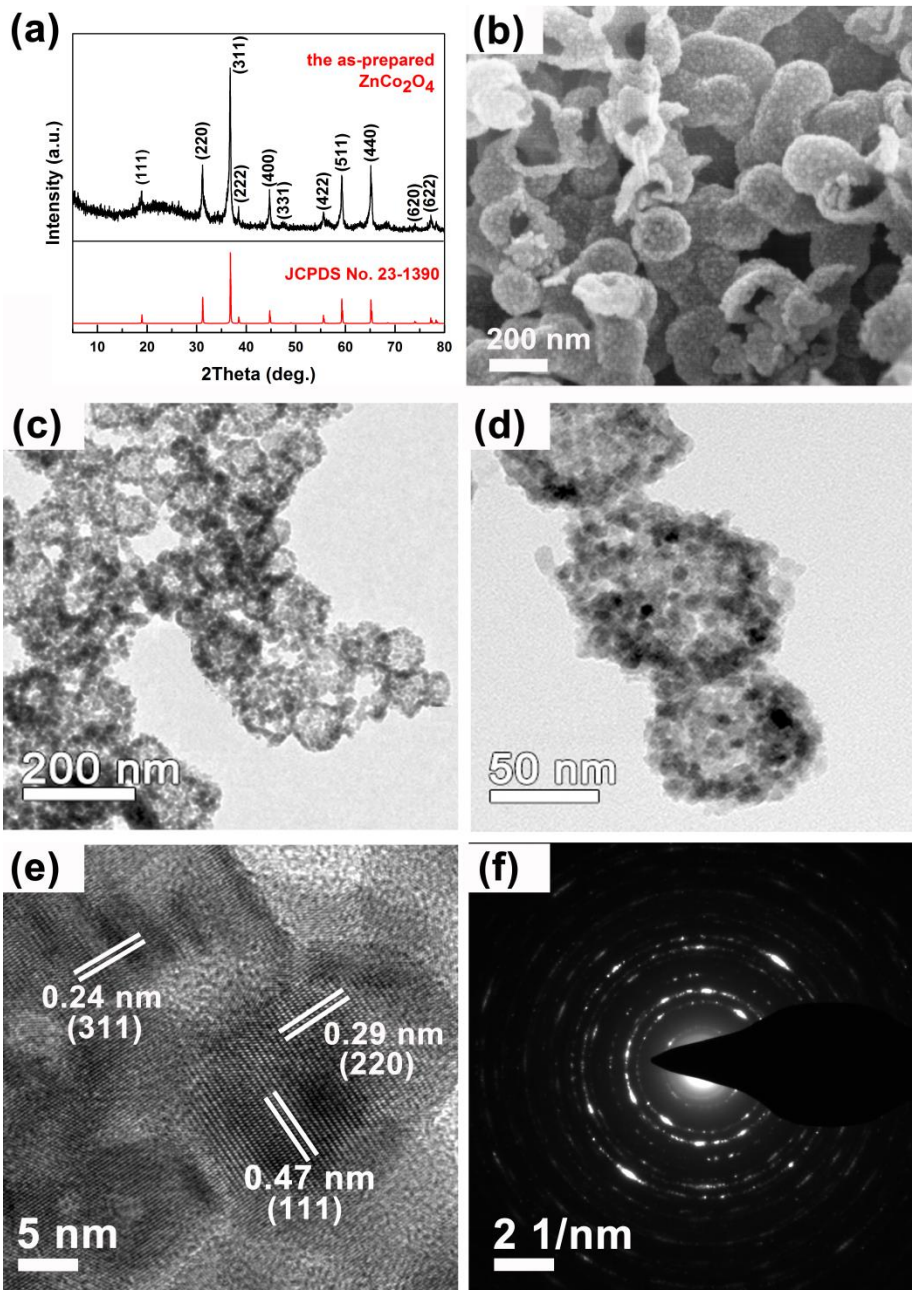

Figure 1. (a) XRD pattern, (b) SEM image, (c, d) low-magnification TEM images, (e) HRTEM image and (f) corresponding SAED pattern of the as-prepared porous $ZnCo_2O_4$ hollow spheres.

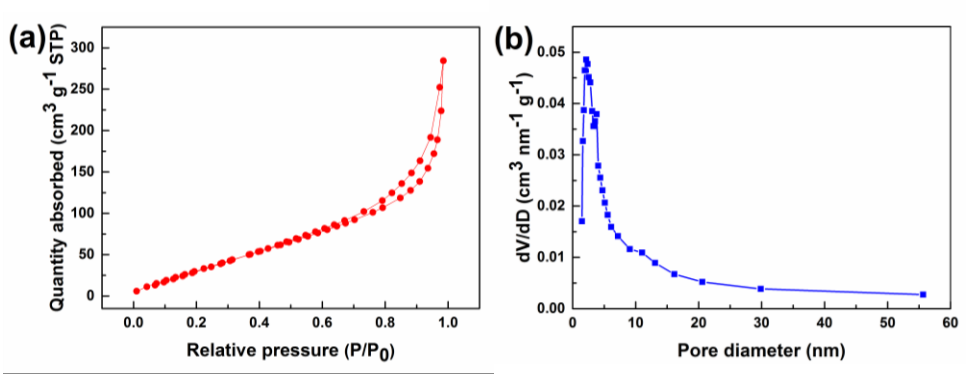

Figure 2. (a) Nitrogen adsorption-desorption isotherm and (b) the corresponding pore size distribution of the as-prepared porous $ZnCo_2O_4$ hollow spheres.

Figure 3a shows the XRD pattern of the as-obtained $NiFe_2O_4$ hollow spheres. It can be seen that all the diffraction peaks can be indexed to cubic $NiFe_2O_4$ phase with the lattice constants of a = b = c = 8.339 Å (space group Fd3m, JCPDS 10-325), without any detectable impurity. An SEM image (Figure 3b) reveals the high quality of the homogeneous and uniform $NiFe_2O_4$ hollow spheres, with a particle size of about 250 nm. The TEM images in Figure 3c and 3d further confirm the hollow and porous structure of the as-prepared $NiFe_2O_4$ sample. The shells of the $NiFe_2O_4$ hollow spheres are about 20 nm in thickness, which are also composed of nanoparticles. HRTEM image (Figure 3e) demonstrates that individual $NiFe_2O_4$ nanoparticle has uniform lattice fringes. The lattice spacing is calculated to be 0.25 nm and 0.29 nm, which agrees well with the (311) and (220) planes of the $NiFe_2O_4$ (JCPDS No. 10-325). The SAED pattern (Figure 3f) shows well-defined rings, indicating that the as-prepared $NiFe_2O_4$ hollow spheres are polycrystalline. Moreover, we have prepared $ZnSnO_3$ (JCPDS No. 28-1486) with porous structure by the same method (Figure 4a). From the SEM, TEM and HRTEM images (Figure 4b-4e), it can be seen that the porous $ZnSnO_3$ is also composed of hollow spheres with thin shells, which are constructed from nanoparticles about 10 nm in diameter. The corresponding SAED pattern (figure 4f) also demonstrates the polycrystalline characteristic of the porous $ZnSnO_3$

hollow spheres. Furthermore, it is found that the obtained $NiFe_2O_4$ and $ZnSnO_3$ hollow spheres both present a pore size distribution ranging from 2 to 5 nm (Figure S5), as well as high surface area of 156.35 m^2 g^{-1} and 137.91 m^2 g^{-1}, respectively.

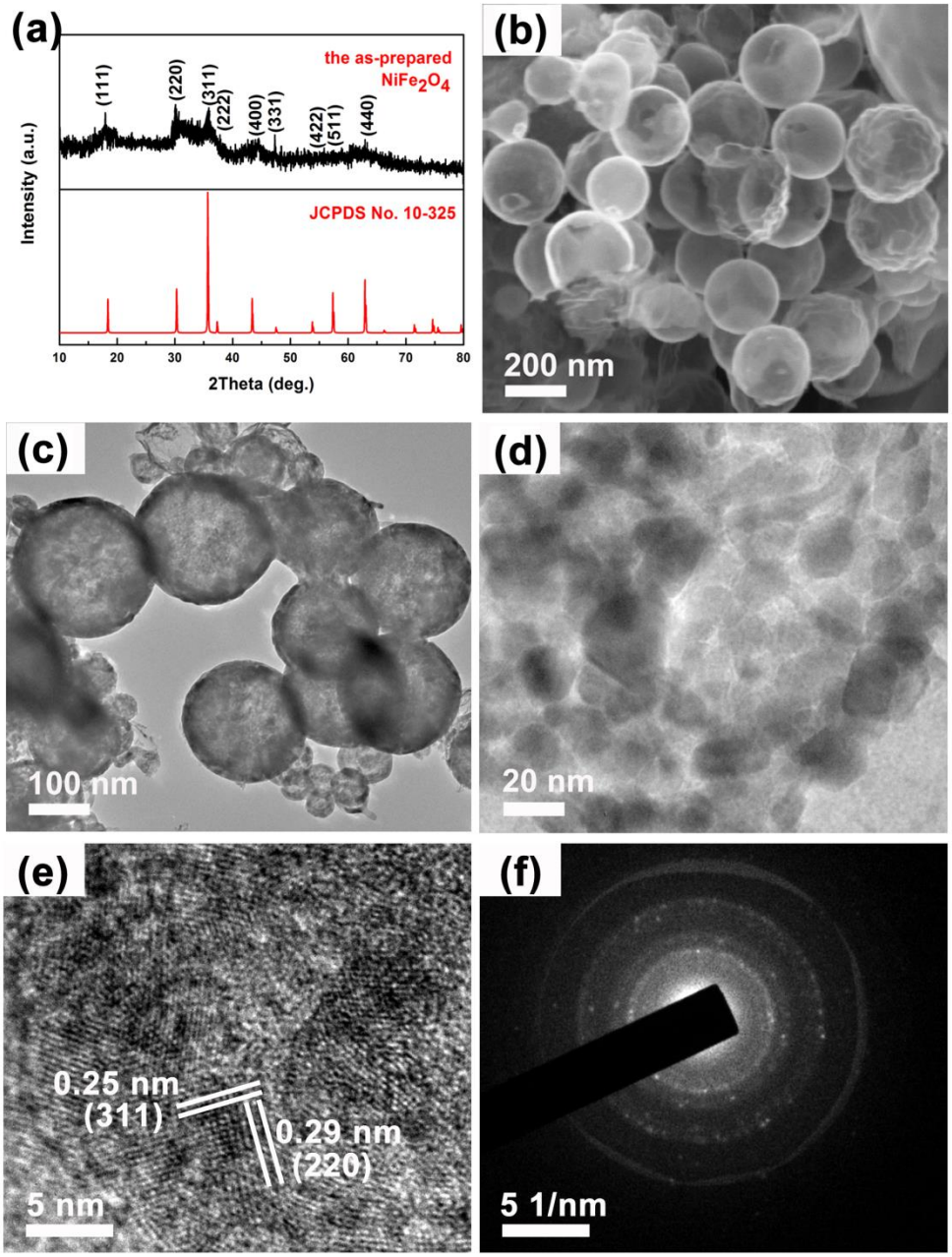

Figure 3. (a) XRD pattern, (b) SEM image, (c, d) low-magnification TEM images, (e) HRTEM image and (f) corresponding SAED pattern of the as-prepared porous $NiFe_2O_4$ hollow spheres.

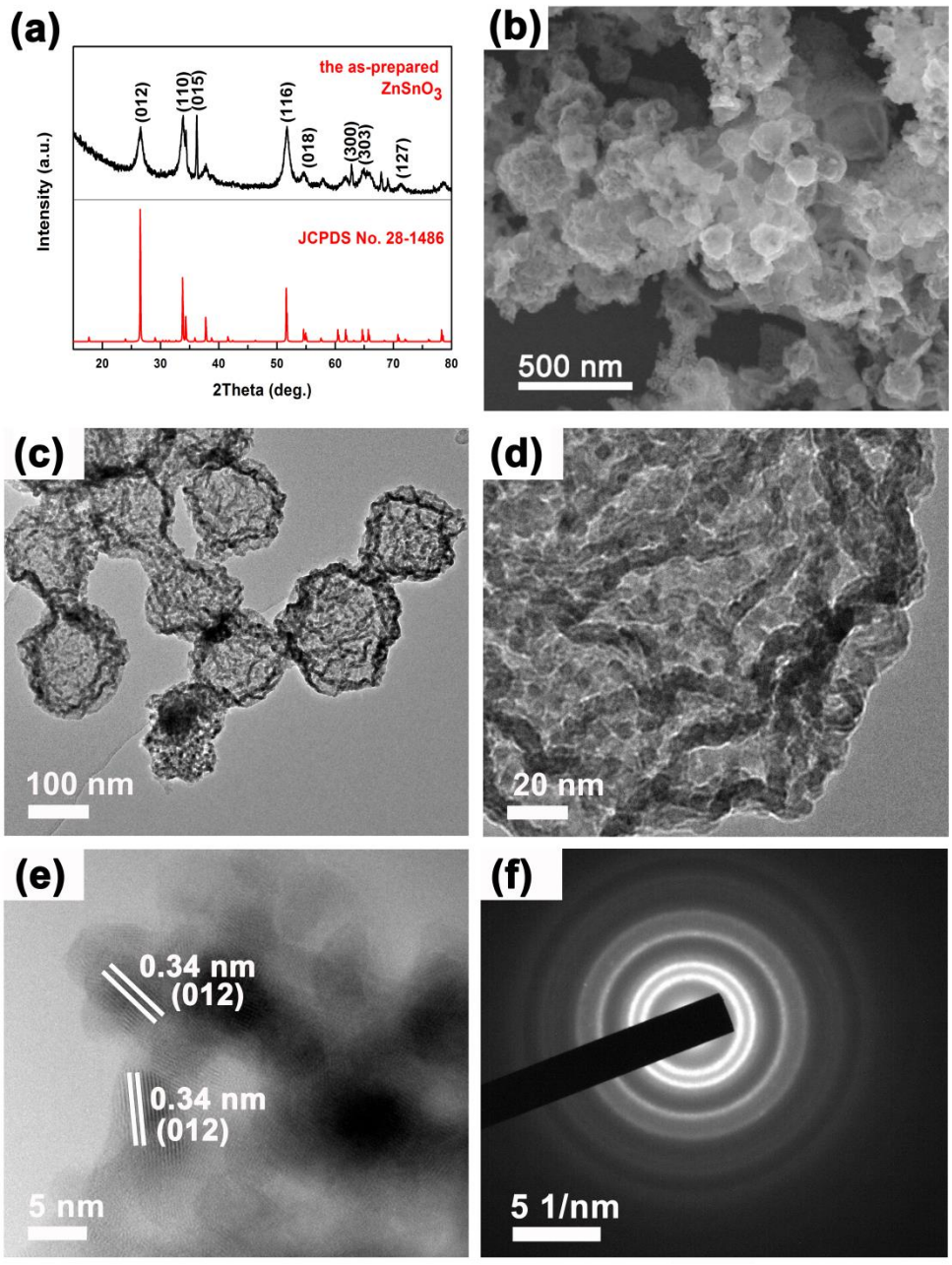

Figure 4. (a) XRD pattern, (b) SEM image, (c, d) low-magnification TEM images, (e) HRTEM image and (f) corresponding SAED pattern of the as-prepared porous $ZnSnO_3$ hollow spheres.

All in all, the MMO samples prepared by this method are composed of small hollow spheres with thin and porous shells, which ensure large electrode/electrolyte contact area, abundant

electroactive sites and fast electron/ion transport rate for electrochemical reactions, demonstrating their potential applications in some novel electronic devices. Herein, the supercapacitive properties of the as-prepared porous $ZnCo_2O_4$, $NiFe_2O_4$ and $ZnSnO_3$ hollow spheres are investigated.

3.2. Supercapacitive performances

The supercapacitive properties of the MMO electrodes were evaluated in a three-electrode configuration. CV and galvanostatic charge-discharge measurements of the $ZnCo_2O_4$ electrode were performed in 2 M KOH. The representative CV profiles of $ZnCo_2O_4$ at different sweep rates of 5~50 mV s^{-1} are shown in Figure 5a. All the CV curves present a pair of well-defined redox peaks, which are distinctly different from those of electrical double layer capacitors (EDLCs), indicating that the electrochemical capacitance mainly originates from Faradaic redox reactions. The reversible conversion in accordance with the well-defined redox peaks may be described as follows:[21,22]

$$Co_2O_4^{2-} + 2H_2O \leftrightarrow 2CoOOH + 2OH^- \quad (4)$$

$$CoOOH + H_2O + e^- \leftrightarrow Co(OH)_2 + OH^- \quad (5)$$

Galvanostatic charge-discharge behaviors of the $ZnCo_2O_4$ material were investigated at different current densities of 1~10 A g^{-1} within 0~0.55 V (vs. Hg/HgO). The nonlinear charge-discharge curves present in Figure 5b clearly demonstrate the occurrence of typical Faradaic redox reactions, further confirming the pseudo-capacitance behavior of the $ZnCo_2O_4$ electrode, which agrees well with the CV results. The specific capacitances calculated from charge-discharge tests are 1158, 1006, 925 and 845 F g^{-1} at 1, 2, 5 and 10 A g^{-1}, respectively (Figure 5c). When the current density increases to 10 A g^{-1}, the capacitance still retains 73% of the capacitance at 1 A g^{-1}. These results suggest good rate capability of the $ZnCo_2O_4$ electrode.

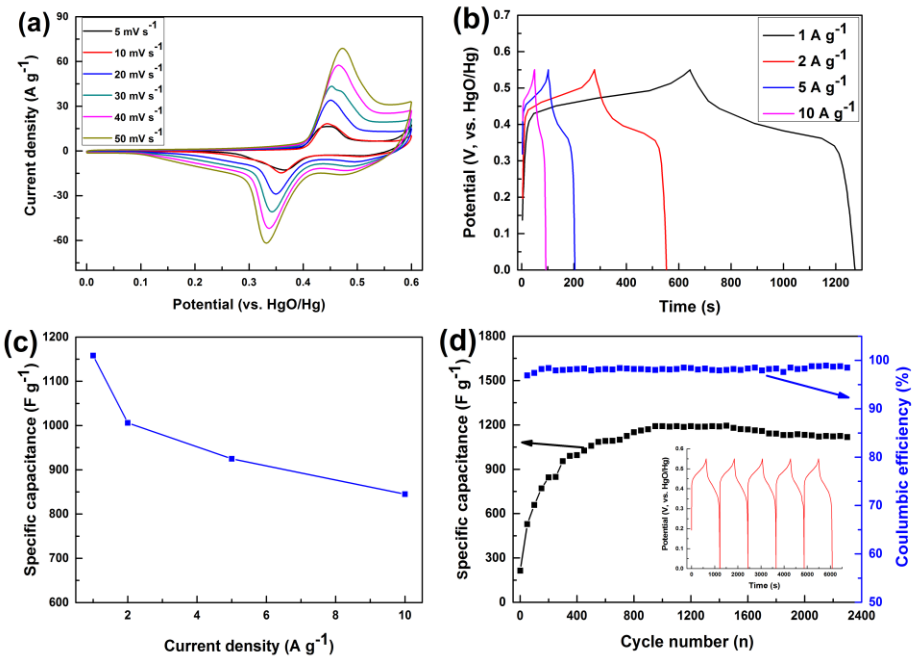

Figure 5. Electrochemical properties of the porous $ZnCo_2O_4$ hollow spheres electrode in a three-electrode measurement system. (a) CV curves at various sweep rates between 0 and 0.6 V (vs. Hg/HgO). (b) Galvanostatic charge-discharge curves with different currents. (c) Specific capacitance as a function of current density. (d) Cycling performance and coulombic efficiency at 1 A g^{-1}. The inset in (d) presents the charge-discharge curves of the last 5 cycles.

Cycling stability and energy deliverable efficiency are also critical parameters for supercapacitors. As shown in Figure 5d, the Coulombic efficiency is as high as 98% even after 2300 charge-discharge cycles, demonstrating excellent kinetic reversibility and good cycling stability of the porous $ZnCo_2O_4$ hollow spheres. It is observed that the discharge specific capacitance gradually increases in the initial 600 cycles. The increase of capacity may be attributed to the activation process for $ZnCo_2O_4$ with high porosity and hollow structure. The highest specific capacitance reaches 1192 F g^{-1}, which still remains 1109 F g^{-1} after 2300 cycles, with a capacitance retention rate of 93.11%. The charge-discharge curves of the last five cycles

have been inserted in Figure 5d. A pair of well-defined charge-discharge plateaus is observed and the curve shapes are similar to those of the initial cycles. The above results further ratify the electrochemical reversibility of the porous $ZnCo_2O_4$ hollow spheres in energy storage applications. Moreover, the as-prepared porous $NiFe_2O_4$ and $ZnSnO_3$ hollow spheres also display promising application as electrode materials for supercapacitors (Figure S6 and S7).

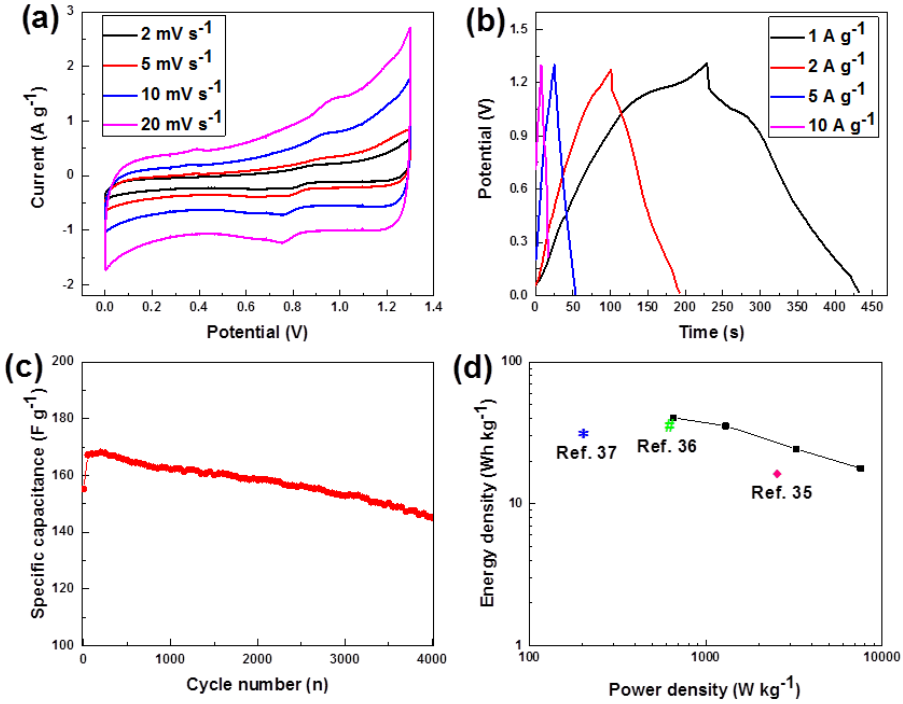

Figure 6. Electrochemical properties of the $ZnCo_2O_4$//AC ASC device. (a) CV curves at various sweep rates with the working potential window of 1.3 V. (b) Galvanostatic charge-discharge curves with different currents. (c) Cycling performance at 1 A g^{-1}. (d) Ragone plots and comparison with the previous reports.

To further evaluate the as-prepared $ZnCo_2O_4$ electrode for practical applications, $ZnCo_2O_4$//AC ASCs are fabricated. The working potential window of the ASC device is 1.3 V in 2 M KOH. Figure 6a shows the CV profiles of the assembled $ZnCo_2O_4$//AC at the scan rates of 2~20 mV s^{-1}.

Each CV curve displays a cathodic peak and an anodic peak, demonstrating the pseudocapacitive property of $ZnCo_2O_4$//AC. Increasing the scan rates, the CV curves are still stable at 20 mV s^{-1}, demonstrating fast charging and discharging characteristics. The galvanostatic charge-discharge testing of the capacitor was conducted with different currents (Figure 6b). The specific capacitance of $ZnCo_2O_4$//AC achieves 167.7 F g^{-1} at 1 A g^{-1} and it still remains 61.5 F g^{-1} at 10 A g^{-1}. Figure 6c shows the cycling stability of $ZnCo_2O_4$//AC at a current density of 1 A g^{-1}. The capacitance retention rate is as high as 86.8% after 4000 cycles. The power performance of $ZnCo_2O_4$//AC is also presented in the Ragone plot. As shown in Figure 6d, the as-prepared $ZnCo_2O_4$//AC delivers an energy density of 39.36 Wh kg^{-1} at a power density of 650 W kg^{-1} and a power density of 7540 W kg^{-1} at an energy density of 17.8 Wh kg^{-1}, which are higher than previously reported $ZnCo_2O_4$ nanowire//AC,[35] $ZnCo_2O_4$@MnO_2//α-Fe_2O_3[36] and $ZnCo_2O_4$/PPy//PPy.[37]

To investigate the structure durability of the as-prepared porous mixed metal oxide hollow spheres, the pristine $ZnCo_2O_4$ electrode and the cycled $ZnCo_2O_4$ electrode are compared in Figure S8. As shown in Figure S8b, after 2000 charge-discharge cycles, the $ZnCo_2O_4$ spheres are not so regular as the pristine electrode, but the sphere-like shape is still maintained well. TEM image shown in Figure S8c demonstrates that even after 2000 cycle at 1 A g^{-1}, the $ZnCo_2O_4$ material is still of hollow structure composed of nanoparticles without aggregation, further confirming the good stability of the porous hollow spheres. The good electrochemical properties of the as-prepared $ZnCo_2O_4$ hollow spheres may be due to their following merits: on one hand, the small size, hollow structure, high porosity and ultrathin shells could provide the $ZnCo_2O_4$ material with a large surface area, which implies a large contact area for electrode and electrolyte, and abundant electroactive sites for the redox reactions. On the other hand, they effectively help

to accelerate the transportation/diffusion of electrons and ions, implying fast kinetics. Furthermore, the cavities resulting from the hollow structure and porous structure could significantly buffer the stress emerged during the electrochemical reaction process. So, their unique structural properties endow the as-obtained $ZnCo_2O_4$ hollow spheres with high discharge capacitance, excellent cycling stability and good rate performance as electrode materials for supercapacitors.

4. CONCLUSIONS

In summary, it has been demonstrated that the "ion adsorption-annealing" technique is very effective for synthesizing porous mixed metal oxide hollow spheres with ultrathin shells and high porosity. The unique structure is favorable for sufficient contact between electrode/electrolyte interfaces, thus provide abundant electrochemically active sites and fast electron and electrolyte ion transportation/diffusion. Last but not least, this structure can maintain well during charge-discharge process. The superior electrochemical performance of such porous $ZnCo_2O_4$ hollow spheres suggests that the porous hollow nanostructures, together with the simple synthesis approach are also expected to be useful in designing other high performance energy storage materials.

ASSOCIATED CONTENT

Supporting Information. The Supporting Information is available free of charge via the Internet at http://pubs.acs.org. Figures showing the crystal structure, morphology and thermal properties of the as prepared Zn-Co-CSs precursor, Nitrogen adsorption-desorption isotherm, pore size distribution and supercapcitive properties of $NiFe_2O_4$ and $ZnSnO_3$, the EDS spectrum of $ZnCo_2O_4$ and its morphology after long cycles.

AUTHOR INFORMATION

Corresponding Author

*E-mail: zguo@uow.edu.au (Z. P. Guo)

*E-mail: wangc@jsnu.edu.cn (C. Wang)

Notes

The authors declare no competing financial interest.

ACKNOWLEDGMENT

This work is supported by the National Natural Science Foundation of China (21473081, 21376113) and the Australian Research Council (ARC) (DP1094261 and FT150100109).

REFERENCES

(1) Wang, G.; Zhang, L.; Zhang, J. A Review of Electrode Materials for Electrochemical Supercapacitors. *Chem. Soc. Rev.* **2012,** 41, 797-828.

(2) Ellis, B. L.; Knauth, P.; Djenizian, T. Three-Dimensional Self-Supported Metal Oxides for Advanced Energy Storage. *Adv. Mater.* **2014,** 26, 3368-3397.

(3) Huang G.; Zhang F.; Du X.; Qin Y.; Yin D.; Wang L. Metal Organic Frameworks Route in Situ Insertion of Multiwalled Carbon Nanotubes in Co_3O_4 Polyhedra as Anode Materials for Lithium-Ion Batteries. *ACS Nano* **2015,** 9, 1592-1599.

(4) Xia, X.; Zhang, Y.; Chao, D.; Guan, C.; Zhang, Y.; Li, L.; Ge, X.; Bacho, I. M.; Tu, J.; Fan, H. J. Solution Synthesis of Metal Oxides for Electrochemical Energy Storage Applications. *Nanoscale* **2014,** 6, 5008-5048.

(5) Wu, H.; Lou, Z.; Yang, H.; Shen, G., A Flexible Spiral-Type Supercapacitor Based on $ZnCo_2O_4$ Nanorod Electrodes. *Nanoscale* **2015,** 7, 1921-1926.

(6) Liu, B.; Liu, B.; Wang, Q.; Wang, X.; Xiang, Q.; Chen, D.; Shen, G. New Energy Storage Option: toward $ZnCo_2O_4$ Nanorods/Nickel Foam Architectures for High-Performance Supercapacitors. *ACS Appl. Mater. Interfaces* **2013,** 5, 10011-10017.

(7) Luo, W.; Hu, X.; Sun, Y.; Huang, Y. Electrospun Porous $ZnCo_2O_4$ Nanotubes as a High-Performance Anode Material for Lithium-Ion Batteries. *J. Mater. Chem.* **2012**, 22, 8916-8921.

(8) Yu, Z.; Chen, L.; Yu, S. Growth of $NiFe_2O_4$ Nanoparticles on Carbon Cloth for High Performance Flexible Supercapacitors. *J. Mater. Chem. A* **2014**, 2, 10889-10894.

(9) Cherian, C. T.; Sundaramurthy, J.; Reddy, M. V.; Kumar, P. S.; Mani, K.; Pliszka, D.; Sow, C. H.; Ramakrishna, S.; Chowdari, B. V. R. Morphologically Robust $NiFe_2O_4$ Nanofibers as High Capacity Li-Ion Battery Anode Material. *ACS Appl. Mater. Interfaces* **2013**, 5, 9957-9963.

(10) Wang, Z.; Zhang, X.; Li, Y.; Liu, Z.; Hao, Z. Synthesis of Graphene-$NiFe_2O_4$ Nanocomposites and Their Electrochemical Capacitive Behaviour. *J. Mater. Chem. A* **2013**, 1, 6393-6399.

(11) Han, F; Li, W; Lei, C; He, B; Oshida, K; Lu A. Selective Formation of Carbon-Coated, Metastable Amorphous $ZnSnO_3$ Nanocubes Containing Mesopores for Use as High-Capacity Lithium-Ion Battery. *Small* **2014**, 10, 2637-2644.

(12) Hong, Y. J.; Kang, Y. C. Formation of Core-Shell-Structured Zn_2SnO_4-Carbon Microspheres with Superior Electrochemical Properties by One-Pot Spray Pyrolysis. *Nanoscale* **2015**, 7, 701-707.

(13) Yuan, C.; Wu, H. B.; Xie, Y.; Lou, X. W. Mixed Transition-metal Oxides: Design, Synthesis, and Energy-Related Applications. *Angew. Chem., Int. Ed.* **2014**, 53, 1488-1450.

(14) Sharma, Y.; Sharma, N.; Rao, G. V. S.; Chowdari, B. V. R. Nanophase $ZnCo_2O_4$ as a High Performance Anode Material for Li-Ion Batteries, *Adv. Funct. Mater.* **2007**, 17, 2855-2861.

(15) Guo, L.; Ru, Q.; Song, X.; Hu, S.; Mo, Y. Mesoporous $ZnCo_2O_4$ Microspheres as an Anode Material for High-Performance Secondary Lithium Ion Batteries. *RSC Adv.* **2015**, 5, 19241-19247.

(16) Liu, X.; Shi, S.; Xiong, Q.; Li, L.; Zhang, Y.; Tang, H.; Gu, C.; Wang, X.; Tu, J. Hierarchical $NiCo_2O_4$@$NiCo_2O_4$ Core/Shell Nanoflake Arrays as High-Performance Supercapacitor Materials. *ACS Appl. Mater. Interfaces* **2013**, 5, 8790-8795.

(17) Wang, Q.; Du, J.; Zhu, Y.; Yang, J.; Chen, J.; Wang, C.; Li, L.; Jiao, L. Facile Fabrication and Supercapacitive Properties of Mesoporous Zinc Cobaltite Microspheres. *J. Power Sources* **2015,** 284, 138-145.

(18) Qiu, Y.; Yang, S.; Deng, H.; Jin, L.; Li, W. A Novel Nanostructured Spinel $ZnCo_2O_4$ Electrode Material: Morphology Conserved Transformation from A Hexagonal Shaped Nanodisk Precursor and Application in Lithium Ion Batteries. *J. Mater. Chem.* **2010,** *20*, 4439-4444.

(19) Wang, Q.; Zhu, L.; Sun, L.; Liu, Y.; Jiao, L. Facile synthesis of hierarchical porous $ZnCo_2O_4$ microspheres for high-performance supercapacitors. *J. Mater. Chem. A* **2015,** 3, 982-985.

(20) Chen, Y.; Qu, B.; Mei, L.; Lei, D.; Chen, L.; Li, Q.; Wang, T. Synthesis of $ZnSnO_3$ Mesocrystals from Regular Cube-Like to Sheet-Like Structures and Their Comparative Electrochemical Properties in Li-Ion Batteries. *J. Mater. Chem.* **2012**, 22, 25373-25379.

(21) Bao, F.; Wang, X.; Zhao, X.; Wang, Y.; Ji, Y.; Zhang, H.; Liu, X. Controlled Growth of Mesoporous $ZnCo_2O_4$ Nanosheet Arrays on Ni Foam as High-Rate Electrodes for Supercapacitors. *RSC Adv.* **2014,** 4, 2393-2397.

(22) Wang, S.; Pu, J.; Tong, Y.; Cheng, Y.; Gao, Y.; Wang, Z. $ZnCo_2O_4$ Nanowire Arrays Grown on Nickel Foam for High-Performance Pseudocapacitors. *J. Mater.Chem. A* **2014,** 2, 5434-5440.

(23) Cheng, J.; Lu, Y.; Qiu, K.; Yan, H.; Hou, X.; Xu, J.; Han, L.; Liu, X.; Kim, J. K.; Luo, Y. Mesoporous $ZnCo_2O_4$ Nanoflakes Grown on Nickel Foam as Electrodes for High Performance Supercapacitors. *Phys. Chem. Chem. Phys.* **2015,** 17, 17016-17022.

(24) Ge, J.; Fan, G.; Si, Y.; He, J.; Kim, H.; Ding, B.; Al-Deyab, S. S.; El-Newehy, M.; Yu, J. Elastic and Hierarchical Porous Carbon Nanofibrous Membranes Incorporated with $NiFe_2O_4$ Nanocrystals for Highly Efficient Capacitive Energy Storage. *Nanoscale* **2016**, 8, 2195-2204.

(25) Liu, B.; Wang, X.; Liu, B.; Wang, Q.; Tan, D.; Song, W.; Hou, X.; Chen, D.; Shen, G. Advanced Rechargeable Lithium-Ion Batteries Based on Bendable $ZnCo_2O_4$-Urchins-on-Carbon-Fibers Electrodes. *Nano Res.* **2013,** 6, 525-534.

(26) Deng, Y.; Zhang, Q.; Tang, S.; Zhang, L.; Deng, S.; Shi, Z.; Chen, G. One-Pot Synthesis of $ZnFe_2O_4$/C Hollow Spheres as Superior Anode Materials for Lithium Ion Batteries. *Chem. Commun.* **2011,** 47, 6828-6830.

(27) Lou, X. W.; Lynden A, A.; Yang, Z. Hollow Micro-/Nanostructures: Synthesis and Applications. *Adv. Mater.* **2008,** 20, 3987-4019.

(28) Hu, J.; Chen, M.; Fang, X.; Wu, L. Fabrication and Application of Inorganic Hollow Spheres. *Chem. Soc. Rev.* **2011,** 40, 5472-5491.

(29) Guo, H.; Li, T.; Chen, W.; Liu, L.; Yang, X.; Wang, Y.; Guo, Y., General Design of Hollow Porous $CoFe_2O_4$ Nanocubes from Metal-Organic Frameworks with Extraordinary Lithium Storage. *Nanoscale* **2014,** 6, 15168-15174.

(30) Lai, X.; Halpert, J. E.; Wang, D. Recent Advances in Micro-/Nano-Structured Hollow Spheres for Energy Applications: from Simple to Complex Systems. *Energy Environ. Sci.* **2012,** 5, 5604-5618.

(31) Wang, J.; Yang, N.; Tang, H.; Dong, Z.; Jin, Q.; Yang, M.; Kisailus, D.; Zhao, H.; Tang, Z.; Wang, D. Accurate Control of Multishelled Co_3O_4 Hollow Microspheres as High-Performance Anode Materials in Lithium-Ion Batteries. *Angew. Chem., Int. Ed.* **2013**, 52, 6417-6420.

(32) Zhang, G.; Lou, X. General Synthesis of Multi-Shelled Mixed Metal Oxide Hollow Spheres with Superior Lithium Storage Properties. *Angew. Chem*. **2014**, 126, 9187-9190.

(33) Tian, Z.; Zhou, Y.; Li, Z.; Liu, Q.; Zou, Z. Generalized Synthesis of a Family of Multishelled Metal Oxide Hollow Microspheres. *J. Mater. Chem. A* **2013**, 1, 3575-3579.

(34) Maria-Magdalena, T.; Markus, A.; Arne, T. A Generalized Synthesis of Metal Oxide Hollow Spheres Using a Hydrothermal Approach. *Chem. Mater.* **2006,** 18, 3808-3812.

(35) Guan, B.; Guo, D.; Hu, L.; Zhang, G.; Fu, T.; Ren, W.; Li, J.; Li, Q. Facile Synthesis of $ZnCo_2O_4$ Nanowire Cluster Arrays on Ni Foam for High-Performance Asymmetric Supercapacitors. *J. Mater. Chem. A* **2014**, 2, 16116-16123.

(36) Ma, W.; Nan, H.; Gu, Z.; Geng, B.; Zhang, X. Superior Performance Asymmetric Supercapacitors Based on $ZnCo_2O_4$@MnO_2 Core-Shell Electrode. *J. Mater. Chem. A* **2015**, 3, 5442-5448.

(37) Chen, T.; Fan, Y.; Wang, G.; Yang, Q.; Yang, R. Rationally Designed Hierarchical $ZnCo_2O_4$/Polypyrrole Nanostructures for High-Performance Supercapacitor Electrodes. *RSC Adv.* **2015**, 5, 74523-74530.

Table of Contents Graphic

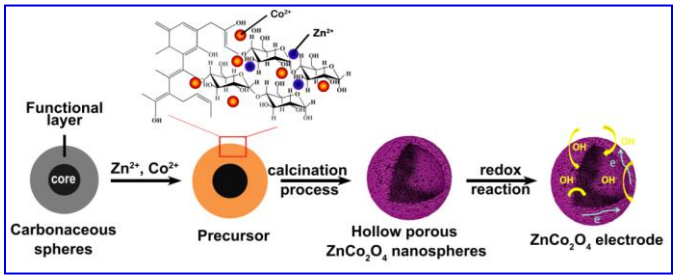

Supporting Information

General Synthesis of Porous Mixed Metal Oxide Hollow Spheres with Enhanced Supercapacitive Properties

Qinghong Wang,[a, b] Yuxuan Zhu,[a] Jing Xue,[a] Xinsheng Zhao,[c] Zaiping Guo,[b,*] Chao Wang[a,*]

[a] School of Chemistry and Chemical Engineering, Jiangsu Key Laboratory of Green Synthetic Chemistry for Functional Materials, Jiangsu Normal University, Xuzhou, Jiangsu 221116, China. Email: wangc@jsnu.edu.cn

[b] Institute for Superconducting & Electronic Materials, University of Wollongong, Wollongong, NSW 2522, Australia. Email: zguo@uow.edu.au

[c] Hydrogen energy laboratory, School of Physics and Electronic Engineering, Jiangsu Normal University, Xuzhou, Jiangsu 221116, China

Figure S1. XRD patterns of carbohydrate spheres and the Zn-Co-CSs precursor.

Figure S2. (a, b) SEM images of carbohydrate spheres; (c, d) SEM images of the Zn-Co-CSs precursor.

Figure S3. TGA curve of the Zn-Co-CSs precursor.

Figure S4. EDS spectrum of the as-prepared porous $ZnCo_2O_4$ hollow spheres.

Figure S5. Nitrogen adsorption-desorption isotherm and the corresponding pore size distribution of the as-prepared samples: (a, b) porous $NiFe_2O_4$hollow spheres, (c, d) $ZnSnO_3$ hollow spheres.

Figure S6. Electrochemical properties of the porous $NiFe_2O_4$ hollow spheres electrode: (a) CV curves at different scan rates, (b) galvanostatic charge-discharge curves at different current densities, (c) rate performance, and (d) cycle life. The inset of is the charge-discharge curves of the last 5 cycles.

Figure S7. CV curves of $ZnSnO_3$ electrode at different scan rates in 1 M Na_2SO_4 aqueous electrolyte.

Figure S8. (a) SEM image of the pristine $ZnCo_2O_4$ electrode, (b) SEM image and (c) TEM image of the cycled $ZnCo_2O_4$ electrode after 2000 cycles at 1 A g^{-1}.

Supercapacitive properties of the as-prepared $NiFe_2O_4$ electrode and $ZnSnO_3$ electrode

The capacitive performance of the as-obtained $NiFe_2O_4$ and $ZnSnO_3$ hollow spheres were also investigated in three-electrode system in 2 M KOH and 1 M Na_2SO_4 aqueous electrolyte, respectively. From Figure S6a, it can be seen that the voltammetric currents of $NiFe_2O_4$ electrode increase with the scan rate, showing the behavior similar to that of an ideal capacitor.[1] The specific capacitances were calculated from the corresponding galvanostatic discharge curves (Figure S6b) in the range of -1.0 V to 0 V at various current densities. The values of specific capacitances for $NiFe_2O_4$ composite are 220.1 F g^{-1} at 1 A g^{-1}, 186.7 F g^{-1} at 2 A g^{-1}, 137.9 F g^{-1} at 5 A g^{-1} and 134.6 F g^{-1} at 10 A g^{-1}, respectively. The cycle stability of the as-prepared $NiFe_2O_4$ electrode was tested by performing continuous charge-discharge cycles at a constant discharge current density of 1 A g^{-1}. As shown in Figure S6d, the $NiFe_2O_4$ electrode shows high specific capacitance of 262.2 F g^{-1} and it still remains 181.7 F g^{-1} after 2000 cycles, with the capacity retention rate of 69.4%, showing good cycle stability of the as-prepared $NiFe_2O_4$.

Figure S7 shows that the electrochemical behavior of $ZnSnO_3$ electrode is also similar to ideal capacitor and it delivers specific capacitance of 58.6 F g^{-1} at 5 mV s^{-1}, 35.5 F g^{-1} at 10 mV s^{-1} and 25.2 F g^{-1} at 20 mV s^{-1}.

[1] Kumbhar, V.S.; Jagadale, A.D.; Shinde, N.M.; Lokhande, C.D. Chemical synthesis of spinel cobalt ferrite ($CoFe_2O_4$) nano-flakes for supercapacitor application. *Appl. Surf. Sci.* **2012**, 259, 39-43.

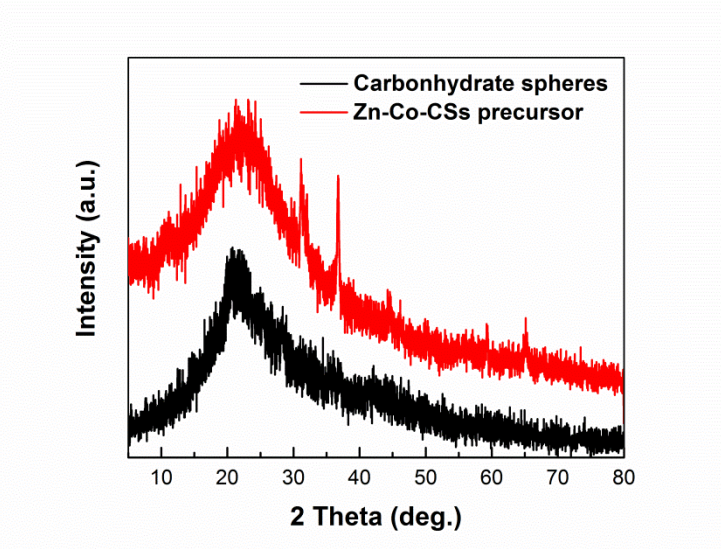

Figure S1. XRD patterns of carbohydrate spheres and the Zn-Co-CSs precursor.

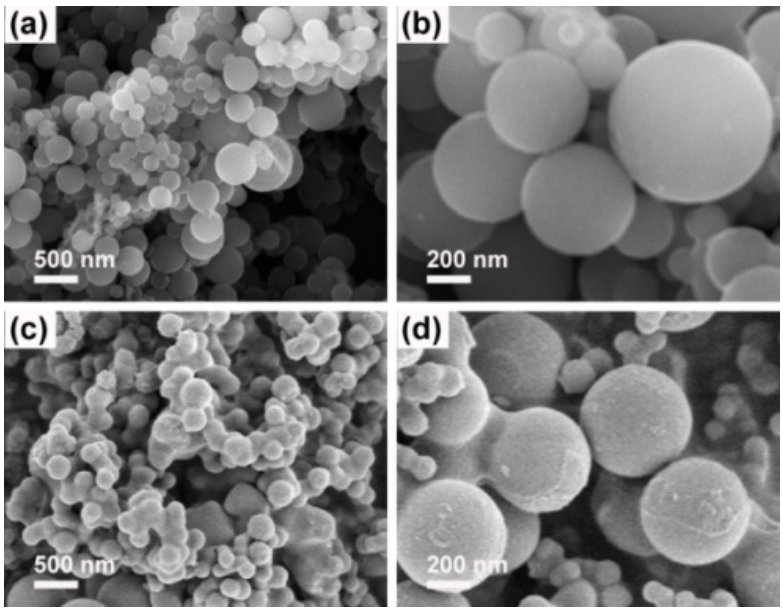

Figure S2. (a, b) SEM images of carbohydrate spheres; (c, d) SEM images of the Zn-Co-CSs precursor.

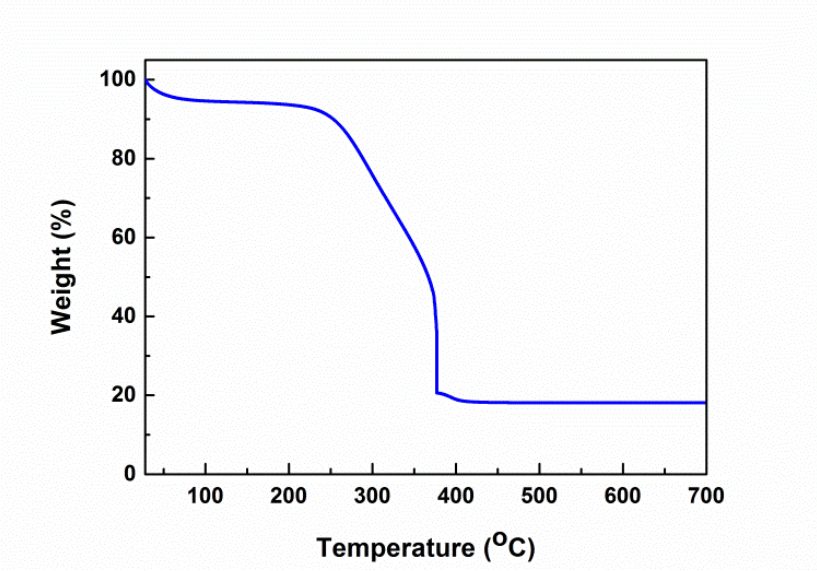

Figure S3. TGA curve of the Zn-Co-CSs precursor.

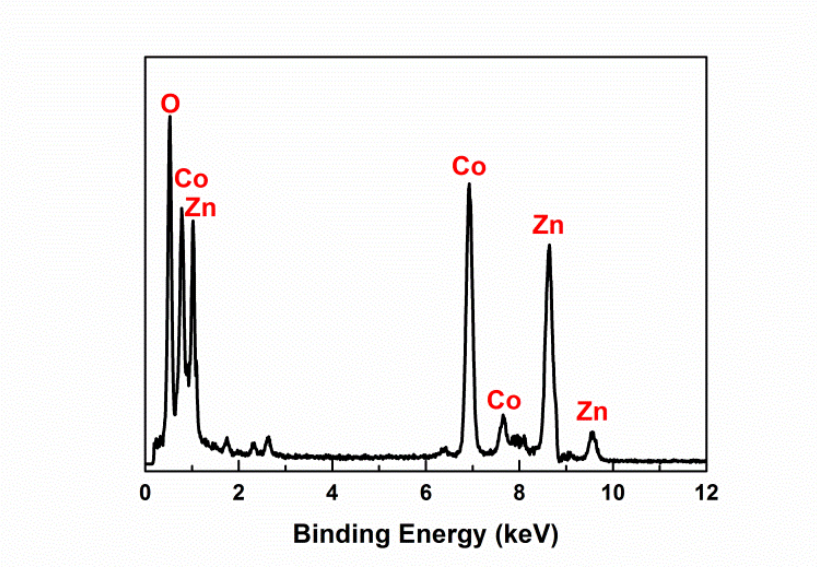

Figure S4. EDS spectrum of the as-prepared porous $ZnCo_2O_4$ hollow spheres.

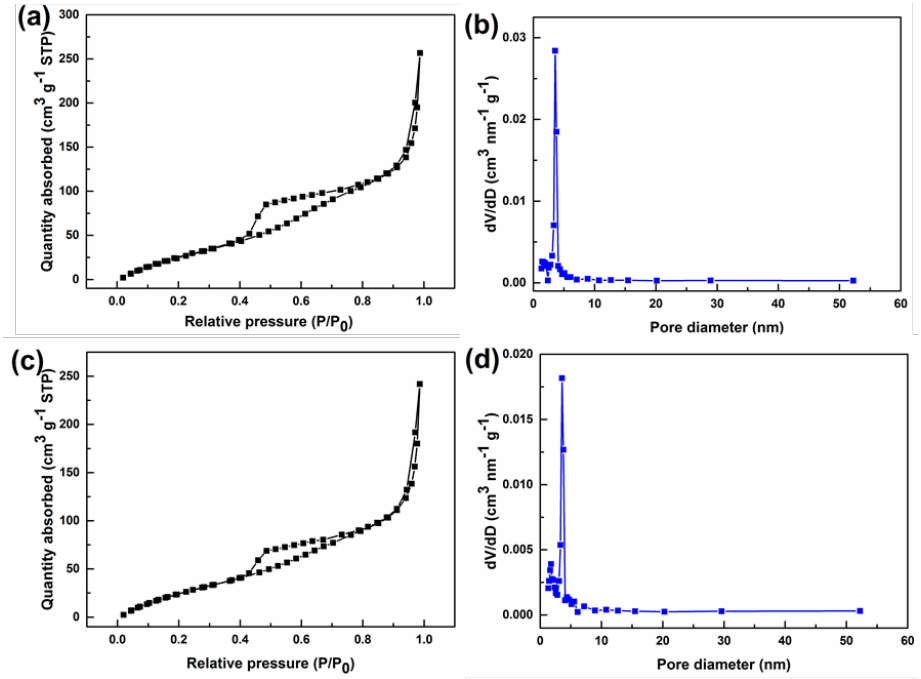

Figure S5. Nitrogen adsorption-desorption isotherm and the corresponding pore size distribution of the as-prepared samples: (a, b) porous $NiFe_2O_4$hollow spheres, (c, d) $ZnSnO_3$ hollow spheres.

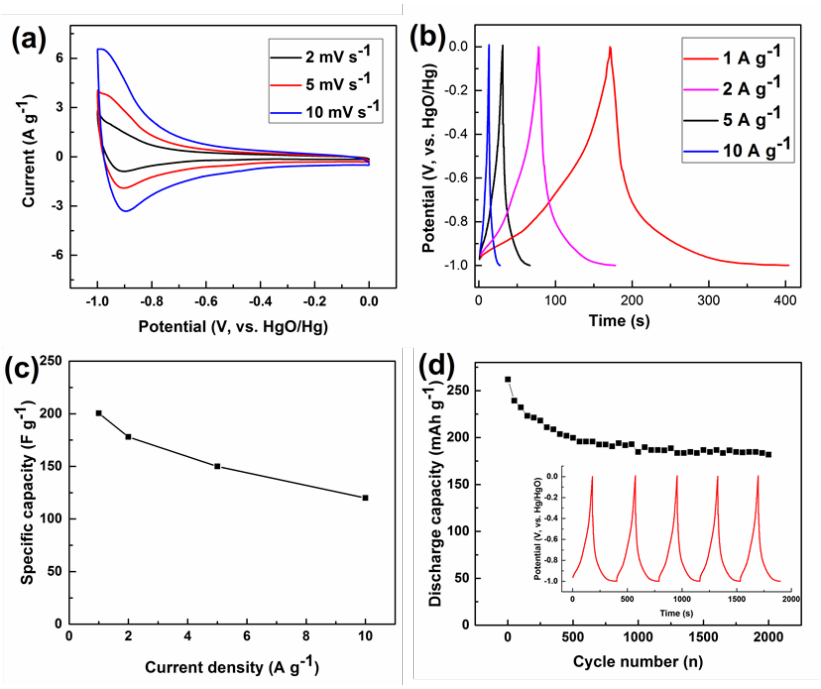

Figure S6. Electrochemical properties of the porous $NiFe_2O_4$ hollow spheres electrode: (a) CV curves at different scan rates, (b) galvanostatic charge-discharge curves at different current densities, (c) rate performance, and (d) cycle life. The inset of is the charge-discharge curves of the last 5 cycles.

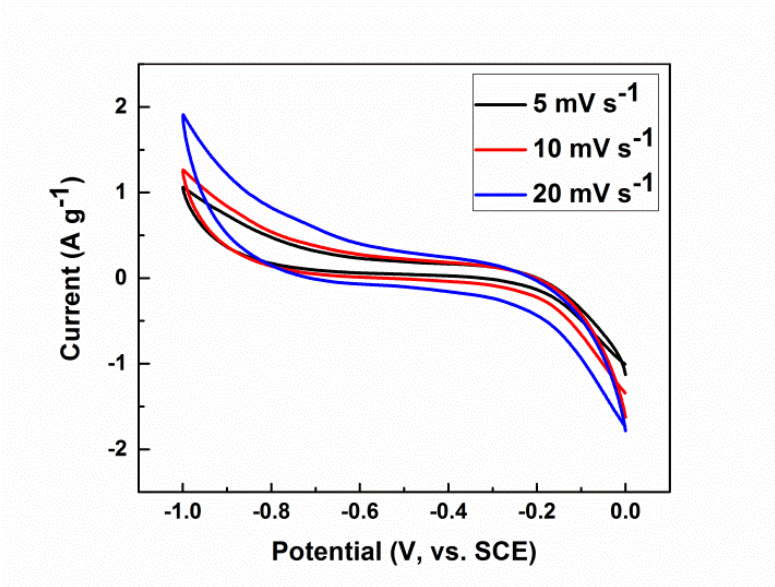

Figure S7. CV curves of $ZnSnO_3$ electrode at different scan rates in 1 M Na_2SO_4 aqueous electrolyte.

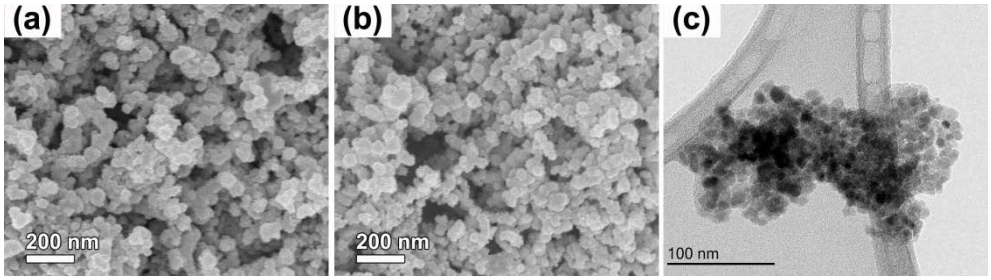

Figure S8. (a) SEM image of the pristine $ZnCo_2O_4$ electrode, (b) SEM image and (c) TEM image of the cycled $ZnCo_2O_4$ electrode after 2000 cycles at 1 A g^{-1}.